# Coupling of the fusion and budding of giant phospholipid vesicles containing macromolecules

Hidetoshi Terasawa[a], Kazuya Nishimura[a], Hiroaki Suzuki[a,b], Tomoaki Matsuura[b,c], and Tetsuya Yomo[a,b,d,1]

[a]Department of Bioinformatic Engineering, Graduate School of Information Science and Technology, Osaka University, Yamadaoka 1-5, Suita, Osaka 565-0871, Japan; [b]Exploratory Research for Advanced Technology, Japan Science and Technology Agency, Yamadaoka 1-5, Suita, Osaka 565-0871, Japan; [c]Department of Biotechnology, Graduate School of Engineering, Osaka University, Yamadaoka 2-1, Suita, Osaka 565-0871, Japan; and [d]Department of Frontier Biosciences, Graduate School of Frontier Biosciences, Osaka University, Yamadaoka 1-5, Suita, Osaka 565-0871, Japan

Edited by Jack W. Szostak, Howard Hughes Medical Institute and Massachusetts General Hospital, Boston, MA, and approved February 22, 2012 (received for review December 9, 2011)

**Mechanisms that enabled primitive cell membranes to self-reproduce have been discussed based on the physicochemical properties of fatty acids; however, there must be a transition to modern cell membranes composed of phospholipids [Budin I, Szostak JW (2011) *Proc Natl Acad Sci USA* 108:5249–5254]. Thus, a growth-division mechanism of membranes that does not depend on the chemical nature of amphiphilic molecules must have existed. Here, we show that giant unilamellar vesicles composed of phospholipids can undergo the coupled process of fusion and budding transformation, which mimics cell growth and division. After gaining excess membrane by electrofusion, giant vesicles spontaneously transform into the budded shape only when they contain macromolecules (polymers) inside their aqueous core. This process is a result of the vesicle maximizing the translational entropy of the encapsulated polymers (depletion volume effect). Because the cell is a lipid membrane bag containing highly concentrated biopolymers, this coupling process that is induced by physical and nonspecific interactions may have a general importance in the self-reproduction of the early cellular compartments.**

protocell | self-division | entropy-driven transformation

It is believed that all modern living organisms originated from a primitive molecular aggregate, termed a protocell, through successive growth and division processes (1, 2). However, it is unlikely that protocells possessed the sophisticated regulatory mechanisms that modern cells have. This riddle has challenged researchers to artificially synthesize a model cell system that could undergo growth and division using a simple set of molecular components (3–5). Various physicochemical phenomena that can mimic essential cellular behaviors have been demonstrated experimentally.

In particular, vesicles consisting of fatty acids have been investigated extensively as a model of a protocell membrane (6–9) because fatty acids are considered to have existed in the prebiotic world (10–12). Spontaneous uptake of micelles of fatty acids into preexisting vesicles, which increases the size of a vesicle, is often modeled as a primitive growth mechanism (7, 13). In combination with mechanical shear-inducing division (fragmentation), fatty acid vesicles have been shown to undergo growth and division under certain experimental conditions (6, 14). Similar uptake of amphiphilic membrane components, followed by the spontaneous birthing of daughter vesicles, has been demonstrated using a set of chemically synthesized molecules (15–17). The key aspect in these systems is that the amphiphilic membrane components are efficiently incorporated due to their physicochemical natures or via chemical conversion.

In the mean time, the membranes of modern living cells are mainly composed of phospholipids, and a plausible scenario of the transition was proposed recently (18). From a physical viewpoint, the typical phospholipids in the cell membrane have much lower critical micelle concentrations (on the order of nanomolar) than that of fatty acids (tens of millimolars) (9), which indicates that phospholipid bilayer membranes are stable over a wide range of amphiphile concentrations, pH, and temperature. Thus, spontaneous incorporation of lipids is unlikely. Before a protocell obtained an ability to synthesize lipids on its own, the vesicle size increase could be achieved by vesicle-to-vesicle fusion initiated by various external stimuli (19–22) or surface functionalization (23–26). Thus, it is conceivable that membrane fusion could be one of the primitive growth pathways for protocells composed of phospholipids. Interestingly, it is speculated that vesicle fusion not only increased the membrane but also supplied reaction substrates with low membrane permeability to increase the molecular complexity of the protocell (27). Division (also referred to as fission or budding) of phospholipid vesicles has also been demonstrated to occur under various conditions, such as mechanical shearing (6, 14, 28, 29), temperature changes (30), addition of monoacyl lipids (31), phase separation (32–34), and digestion of lipid molecules in the internal leaflet (35). Despite these evidences, the coupled growth and division of phospholipid vesicles have not been realized because these processes take place under different conditions. A good combination of external stimuli (energy input) and spontaneous transition must be found to propose a possible pathway of proliferation of the lipid-based protocell.

In the present study, we show that the coupling of growth and division processes of giant unilamellar vesicles (GUVs) composed of phospholipids can be achieved by electrofusion and the spontaneous budding transformation that follows. We used an electric pulse to fuse GUVs, which could be one of the stimuli to fuse membrane in the prebiotic environment (36). After gaining the excess membrane by fusion, a spontaneous budding transformation was shown to occur. We show that budding can be induced by encapsulating inert polymer molecules, which mimic cytosolic macromolecules. This membrane deformation is driven by maximization of the translational entropy of the polymers in the vesicle (37). The combination of these entirely physical and nonspecific effects enables the recursive cycles of fusion and budding of giant lipid vesicles.

## Results

**Electrofusion of GUVs.** We prepared GUVs with the membrane consisting of 1-palmitoyl-2-oleoyl-sn-glycero-3-phosphocholine (POPC), 1-palmitoyl-2-oleoyl-sn-glycero-3-[phospho-rac-(1-glycerol)] (POPG), and cholesterol at a weight ratio of 18 : 2 : 1 using the water-in-oil (W/O) emulsion transfer method (38, 39), which can produce unilamellar vesicles with defined inner and outer aqueous compositions (38, 40, 41). A small portion of POPG,

Author contributions: H.T., H.S., and T.Y. designed research; H.T. and K.N. performed research; H.T., K.N., H.S., T.M., and T.Y. analyzed data; and H.S. wrote the paper.

The authors declare no conflict of interest.

This article is a PNAS Direct Submission.

Freely available online through the PNAS open access option.

[1]To whom correspondence should be addressed. E-mail: yomo@ist.osaka-u.ac.jp.

This article contains supporting information online at www.pnas.org/lookup/suppl/doi:10.1073/pnas.1120327109/-/DCSupplemental.

a negatively charged lipid, was added to obtain dispersed GUVs by electrostatic repulsion (Fig. S1), whereas it did not alter the electrofusion process described below. We performed electrofusion of GUVs (19) under an optical microscope using a handmade chamber with electrodes mounted on a coverslip (Fig. 1*A*). Application of a 150 V/cm alternating current at 1 MHz aligned GUVs in lines (i.e., the pearl-chain formation), and the following three short pulses (60 μs) at 2 to 6 kV/cm induced vesicle fusion. After fusion, we observed that the internal aqueous contents were mixed rapidly (Fig. 1*B* and Movie S1), confirming that multiple vesicles had fused into a single structure. When the applied voltage of the short pulses increased, the number of vesicles that fused together increased (Fig. S2*A*). For example, at applied voltages of 4 and 6 kV/cm, the probability of fusion in which four and five vesicles became a single vesicle was 18% and 13% of all of the fusion events, respectively. In contrast, no fusion events with more than four vesicles occurred at 2 kV/cm. When multiple vesicles fuse at once, the surface-to-volume ratio increases, which is required for vesicles to have freedom for deformation.

**Vesicle Shape Transformation After Fusion.** We observed fused vesicles after electrofusion. Note that after fusion, no electric signal was applied. When there was no polymer encapsulated in the vesicles, the shape of the outermost membrane after fusion was mostly spherical (Fig. S3*A* and Movie S2). On the contrary, various shapes, such as torus, horseshoe, and elongated tubes, were observed when 3 mM PEG 6000 (2.5%wt/wt) was included in vesicles (Fig. S3*B*). We confirmed that, in both cases, the total aqueous volume was conserved during the fusion process (Figs. S4 and S5). Without PEG, the excess membrane invaginated into the vesicle to form the multivesicular structure as a result of the vigorous electrofusion. However, in the presence of PEG, the extent of membrane invagination was relatively small, causing the excess membrane in the outermost shell to have various shapes.

Then, the shapes of fused vesicles containing PEG often transformed into an elongated shape, and finally resulted in a budded shape after neck formation (Fig. 1 *C*–*F* and Movies S3–S6). This transition occurred typically within 1–10 min, whereas no change was observed for vesicles without PEG (Movie S2). The confocal microscope imaging (Fig. 1 *E* and *F*, and Movies S5 and S6) revealed that the invaginated internal structures appeared right after the electrofusion were absorbed into the outer shell over time. This transition gave rise to a freedom in the outer membrane to deform, resulting finally in budding into multiple vesicles with mostly spherical shapes. Moreover, this shape transformation was not observed when the same concentration of PEG 6000 was present in both inner and outer solutions, or only in the outer solution. This result strongly suggests that budding transformation after vesicle fusion was induced by the PEG encapsulated inside vesicles.

Because PEG is used to induce the fusion of cells and liposomes (22), the physical interaction between PEG and lipid membranes has been studied extensively (42). PEG dissolved in the vesicle suspension interacts with lipid membranes nonspecifically, helping to aggregate vesicles by the depletion of PEG on the membrane surface. Therefore, we hypothesized that the depletion interaction induces the budding transformation. The classical hypothesis describing the depletion interaction suggests that, when polymers and other relatively larger particles (e.g., vesicles) are present in solution, particles aggregate together to reduce the volume around the particles (depletion volume, $V_{dep}$), which is limited by the gyration radius of polymers (43–46). This transition is favored because it increases the volume where polymers are able to move freely ($V_{free} = V_{system} - V_{dep}$), thereby increasing the translational entropy of the system (Fig. 2*A*). In a system consisting of a membrane and the polymer solution on one side and under the constraint that the volume and membrane area are conserved, $V_{dep}$ decreases (in turn $V_{free}$ increases) as the integral of the membrane curvature increases (Fig. 2*B*). Thus, the shapes with positive curvatures are thermodynamically favored if the gain of the entropy (reduction of the free energy) due to the increase of $V_{free}$ overcomes the energy necessary to bend the membrane. Recently, this hypothesis was tested using GUVs containing microbeads (1-μm diameter) at a volume fraction of approximately 50% (37). However, this effect has not been studied with nanometric macromolecules, which are more biolo-

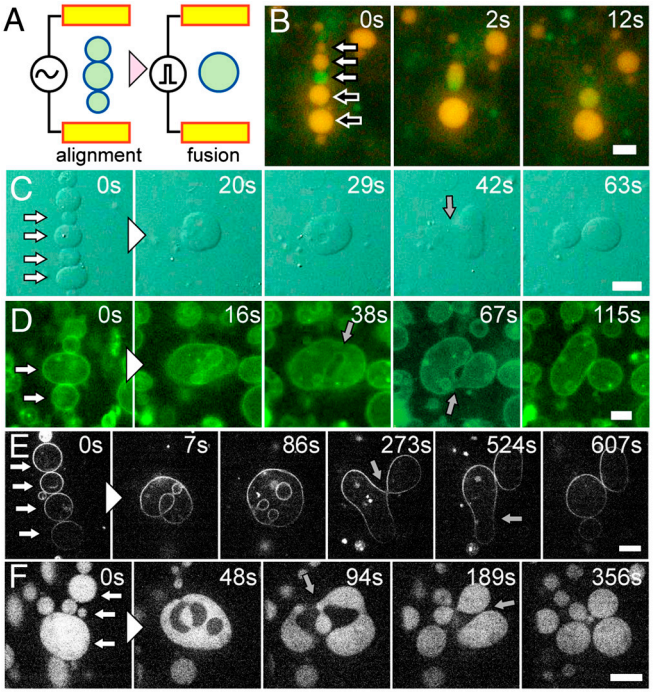


**Fig. 1.** Electrofusion and budding transformation of GUVs. (*A*) Schematic representation of the electrofusion experimental setup. (*B*) Sequential epifluorescence images of the electrofusion of GUVs containing GFP (green) and R-PE (orange) without polymer. White and black-filled arrows at time zero indicate vesicles to fuse together. (*C*–*F*) Sequential images of budding transformations of vesicles containing 3 mM PEG 6000. White-filled arrows at time zero indicate vesicles to fuse together. Gray-filled arrows indicate the neck formation before budding. (*C*) Bright-field images. (*D*) Epifluorescence images of the membrane marked with fluorescence lipids. (*E*) Confocal fluorescence images of the membrane marked with fluorescence lipids. (*F*) Confocal fluorescence images of the vesicles encapsulating FITC-BSA. (Scale bars: 10 μm.)

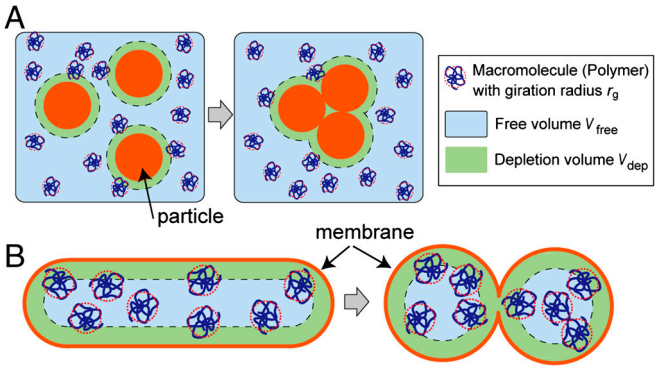


**Fig. 2.** Illustration of the depletion volume effect (not to scale). (*A*) Classical representation of the depletion volume effect. Larger particles in the polymer solution aggregate to reduce $V_{dep}$, in turn increasing $V_{free}$. (*B*) In the system consisting of the GUV containing the polymer, $V_{free}$ increases when the curved area of the membrane increases, under the constraint of constant volume and surface area. Thickness of the polymer depletion volume is exaggerated to clarify the relative difference of $V_{free}$.

gically relevant. We next sought to verify that the budding transformation observed was induced by PEG and dextran as the mimetic materials of cytosolic biopolymers.

**Condition for Budding Transformation.** We examined the extent of this hypothesis by encapsulating PEG 6000 at various concentrations. We evaluated the probability of the budding transformation by observing 50–400 fusion events induced at 6 kV/cm in each PEG concentration. As mentioned previously, the relationship between the volume and surface area is an important parameter in determining vesicle shapes. The reduced volume, $v_{red} = 6\sqrt{\pi}VA^{-3/2}$, where $V$ and $A$ are the volume and surface area of the vesicle, respectively, is often used as an indicator (47, 48). The reduced volume represents the ratio of the vesicle volume to the volume of a sphere with the equivalent surface area ($v_{red} = 1$ for a spherical vesicle and $v_{red} < 1$ for a vesicle with excess membrane area). To correlate this parameter to the probability of budding events, we estimated the $V$ and $A$ of fused vesicles as the sum of those of spherical vesicles before fusion. This evaluation is based on the assumption that these quantities are conserved during fusion and the transformation process, as confirmed by time-lapse 3D image acquisition using confocal microscopy (Fig. S5).

We plotted the probability of budding transformation over the total number of fusion events $P_{bud}(v_{red})$ as a function of $v_{red}$ (Fig. 3*A*). When the concentrations of encapsulated PEG 6000 ($C_{PEG\,6000}$) were 0 and 0.3 mM (0.25%wt/wt), fused vesicles remained spherical, and no budding event was observed. However, at $C_{PEG\,6000} = 1.5$ mM (1.2%wt/wt), the occurrence of the budding events was increased with a negative correlation to $v_{red}$. Also, the budding events became more frequent at higher PEG concentrations. For instance, at $C_{PEG\,6000} = 3$ mM (2.5%wt/wt), the $P_{bud}$ was 20% at $v_{red} \sim 0.7$ but reached approximately 70% at $v_{red} \sim 0.5$. At $C_{PEG\,6000} = 6$ mM (5%wt/wt), $P_{bud}$ reached 100% at $v_{red} = 0.5$. Here we confirmed that the curve of $P_{bud}$ was independent of the applied electric voltage for fusion (Fig. S2*B*). Moreover, similar transformation to the budded shape was confirmed without electrofusion when $v_{red}$ was reduced in the hypertonic condition (Fig. S6). These results support that the budding transformation is not because of the electric pulse applied for fusion. Furthermore, budding transformation was also observed with vesicles prepared by the natural swelling method (Movie S7), confirming that this phenomenon is not specific to the vesicle preparation method that we used. These results support that budding is mainly dependent on the encapsulated PEG molecules and $v_{red}$.

We next examined the dependence of $P_{bud}$ on the molecular weight of the PEG (Fig. 3*B*), because the depletion volume should be proportional to the gyration radius of the polymer (*SI Text*). We found that $P_{bud}$ had a strong positive correlation with the molecular weight. With PEG 400, budding transformation was rarely observed even at the mass concentration (2.5%wt/wt, $C_{PEG\,400} = 62$ mM) where budding occurred with PEG 6000 (2.5%wt/wt, $C_{PEG\,6000} = 3$ mM). In contrast, $P_{bud}$ increased to 100% with PEG 20000 at $C_{PEG\,20000} = 3$ mM. We also examined the effect of a different polymer, dextran (Fig. 3*C*). Although the critical concentration and the molecular weight at which vesicle budding occurs were greater than those of PEG, the identical budding phenomenon was observed. This observation excludes the possibility that budding transformation is only specific to the chemical nature of PEG.

The model based on the depletion volume effect explains the following major characteristics observed. First, at higher concentrations and/or higher molecular weights, budding transformation occurred more rapidly (Fig. S7 and Movie S8). This trend should be because, with a higher free energy difference between the bulk and depletion volume, the membrane continued to maintain its local curvature during fusion, resulting in quick budding transformation. Second, when a greater number of vesicles fused (i.e., $v_{red} < 0.5$), we frequently observed budding into multiple vesicles with nearly spherical shapes (e.g., Fig. 1*F*). We occasionally observed a transformation similar to the pearling instability reported previously (37, 49). This observation is in agreement with the model that budding should continue until $v_{red}$ of each vesicle approaches one, where no excess membrane for deformation remains.

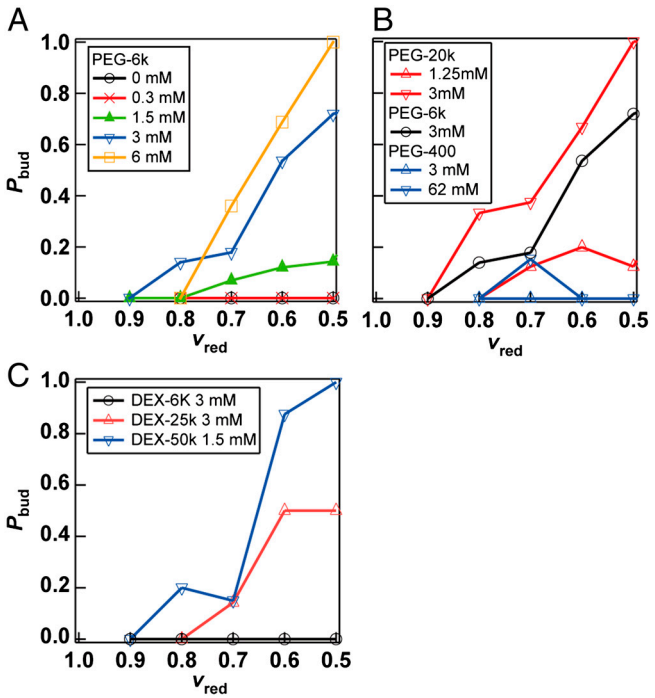


**Fig. 3.** Probability of budding transformation of vesicles encapsulating polymers after electrofusion. (*A*) PEG 6000 at various concentrations. (*B*) PEG with various molecular weight and concentrations. (*C*) Dextran with various molecular weight and concentrations.

**Estimation of the Free Energy.** We performed a simple calculation to determine whether the depletion interaction is the major contribution in the present phenomena. Because the change in depletion volume occurring with the shape transformation is extremely small (the thickness equals the gyration radius of polymers, 1–10 nm), it is difficult to evaluate from the experimentally observed shapes. Thus, we estimated it by approximating the vesicle shapes to mathematically definable geometries (37, 50). In our experiment, we often observed a transformation from the elongated tube to the doublet (budded) shape at the last stage of transformation (Fig. 4*A*). Thus, we approximated these two shapes as a spherocylinder (a cylinder with half-spherical caps at the ends) and two spheres (doublet shape), respectively, and calculated the change in the free energy due to the difference of $V_{dep}$ between the two shapes, $\Delta E_{dep}$ (Fig. 4*B*; see *SI Text* and Table S1 for derivation). Note that in this assumption, $v_{red}$ is approximately 0.7. Here, $\Delta E_{dep}$ was calculated as $\Delta E_{dep} = \Delta\Pi\Delta V_{dep}$, where osmotic pressure of encapsulated polymer $\Delta\Pi$ was experimentally measured by the osmometer. $\Delta V_{dep}$ is a function of the representative vesicle size (e.g., vesicle radius $R$) and the gyration radius of the polymer ($r_g$), which is scaled as $\Delta V_{dep} \propto {r_g}^2 R$. If $|\Delta E_{dep}|$ exceeds the bending energy of a lipid membrane necessary for transformation $|\Delta E_{bend}|$, a doublet shape is thermodynamically preferred, and budding tends to occur. In polymer-encapsulating conditions where the budding transformation occurred in the experiments, [$P_{bud}(v_{red} \leq 0.7) > 0.1$, red bars], the calculated $|\Delta E_{dep}|$ was above $10^{-17}$ J. Mean-

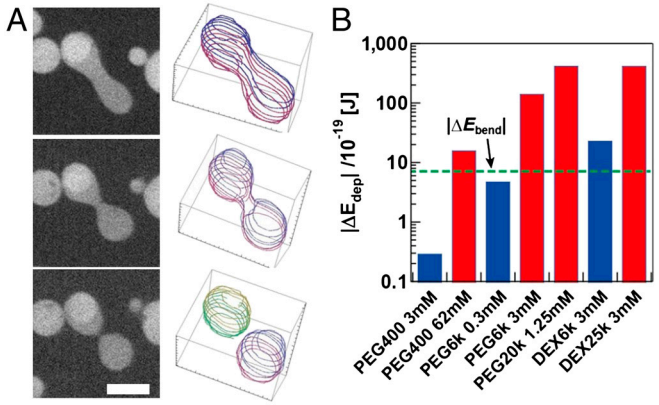


**Fig. 4.** Estimation of the free energy. (*A*) Confocal images and 3D representation of the typical shape transformation at the late phase of budding. Constriction of the elongated shape develops towards budding. (Scale bar: 5 μm.) (*B*) $\Delta E_{dep}$ calculated for the hypothetical transformation from a spherocylinder into two spheres (5-μm diameter was assumed) in various experimental conditions. Red and blue bars, respectively, represent the conditions in which the budding transformation occurred ($P_{bud} > 0.1$) and did not occur ($P_{bud} < 0.1$). The green horizontal line shows the estimated increase of bending energy of the membrane.

while, $|\Delta E_{bend}|$ was derived as a scale-free value of $2\pi\kappa_b(3-\sqrt{3})$, where $\kappa_b$ is the bending coefficient of the lipid membrane. Assuming $\kappa_b \sim 10^{-19}$ J, $|\Delta E_{bend}|$ was estimated to be approximately $10^{-18}$ J, so that the relationship $|\Delta E_{dep}| \gg |\Delta E_{bend}|$ holds due to larger gyration radius and concentration of polymers. In contrast, calculated $|\Delta E_{dep}|$ was smaller than or comparable to $|\Delta E_{bend}|$ in conditions where budding transformation was not observed (blue bars) due to smaller gyration radius and concentration of polymers. Thus, we can conclude that this rough estimation is consistent with the experimental results. Budding transformation was more frequent with PEG than with dextran at an identical molecular weight and concentration because PEG has a greater osmotic activity (22, 51), resulting in a more substantial depletion interaction. Qualitatively, we can extend this discussion for transformations from multivesicular, torus, and horseshoe shapes (Fig. S3*B*) to a budded shape. Because these shapes possess negative curvature when viewed from the side with polymers, the vesicles should transform to increase the area with positive curvature, reducing the depletion volume. Consequently, fused vesicles result in multiple spherical shapes, which have the minimum depletion volume under the constraint of a fixed $v_{red}$.

**Repetitive Cycles of the Fusion and Budding Transformation.** With the present system, the fusion-to-budding transformation can be induced repeatedly by applying an electric signal multiple times (Fig. 5 and Movie S9). Interestingly, this refusion process was induced by applying the 1 MHz, 150 V/cm ac source initially used for the alignment of GUVs, and dc pulses at high voltage were not necessary. The refusion may be facilitated by gentle stimulus due to the attachment of small membrane regions to each other. After the budding transformation, it often remains unclear whether the two vesicles in close proximity are connected or separated (52). We observed the diffusion of the internal aqueous contents from one photobleached vesicle to the neighboring one (Fig. S8). The result indicated that the aqueous volume in budded vesicles remained in separate compartments within the timescale of the experiment (approximately 10 min). Moreover, the budded vesicles occasionally separated as they drifted when there was a convectional flow in the observation chamber (Fig. S9). We assume that the attached part of the membranes may be in a state of hemifusion (22, 53), in which the internal volume is separated into distinct compartments.

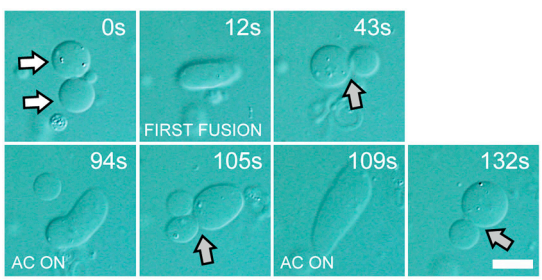


**Fig. 5.** Repetitive cycles of fusion-to-budding transformation. After the first fusion ($t = 12$ s), an ac signal was applied after each budding event ($t = 94$ and 132 s). The vesicles contain 3 mM PEG 6000 (5%wt/wt). White arrows indicate the vesicles to be fused. Gray arrows show the neck formation. (Scale bar: 10 μm.)

## Discussion

In this paper, we demonstrated the coupling of the fusion-to-budding transformation of phospholipid vesicles that mimics the growth and division of protocells using electrofusion and polymer-induced spontaneous vesicle shape transformation. After being elevated to the unstable state by fusion, the vesicle structure returns back to a state similar to the initial condition, which is thermodynamically (entropically) favored. Repetitive cycles were possible under the experimental condition because the constituents in the system remained identical after each cycle. In terms of the membrane physics, the emergence of spontaneous curvature due to the asymmetry of the solute across the membrane was predicted and demonstrated previously (–56), but experimental verification with macromolecules was insufficiently explored. It is worth mentioning that the observed spontaneous transformation was induced by inert macromolecules at a weight concentration of approximately 5%. Because the modern cell contains macromolecules at a concentration of approximately 30% (57), this depletion interaction-based self-division might have had a general influence in the prebiotic-to-modern evolutionary pathway. Indeed, the stimulus required to gain excess membrane is not limited to electrofusion; it could be any energy fluctuation that may have existed in the prebiotic world and/or incorporation by the internal synthesis. Vesicle transformation due to the physical and nonspecific interactions presented in this work serves as an important model for protocell proliferation.

## Materials and Methods

**Materials.** POPC and POPG were purchased from Avanti Polar Lipids. Cholesterol was purchased from Nacalai Tesque. Green fluorescence-tagged lipid 2-(4,4-difluoro-5,7-dimethyl-4-bora-3a,4a-diaza-s-indacene-3-dodecanoyl)-1-hexadecanoyl-*sn*-glycero-3-phosphocholine (BODIPY-HPC), red fluorescent protein R-phycoerythrin (R-PE), and fluorescein conjugated BSA (FITC-BSA) was purchased from Invitrogen. GFP was supplied from the lab stock. PEG and dextran with various molecular weights were purchased from Wako and Sigma Aldrich, respectively. The inner solution encapsulated in the vesicles was an aqueous buffer consisting of 50 mM Hepes-KOH (pH 7.6), 150 mM sucrose, 350 mM glucose, and polymers at various concentrations (0–6%wt/wt). The outer solution of the vesicles was an aqueous buffer consisting of 50 mM Hepes-KOH (pH 7.6) and 500 mM glucose. When the polymer was included in the inner solution, glucose in the outer solution was increased to compensate the osmolarity.

**Preparation of GUVs.** We prepared GUVs with the W/O emulsion transfer method as described previously (39) with slight modifications. POPC, POPG, and cholesterol at the weight ratio of 18:2:1 (total 21 mg) were dissolved in 210 μL of chloroform, and this mixture was mixed with 4.2 mL of liquid paraffin (128-04375; Wako). When visualizing the membrane, BODIPY-HPC was included at a 0.1% molar fraction to POPC. This solution was heated at 80 °C for 20 min to completely dissolve the lipids and evaporate the chloroform. This solution (500 μL) was then transferred to a glass tube, to which 45 μL of the inner solution was added. When visualizing the inner aqueous phase, 15.5 μM GFP, 400 nM R-PE, or 5 μM FITC-BSA was included in the inner solution. This mixture was vortexed for 30 s to form a W/O emulsion that was then equilibrated on ice for 10 min. A 400-μL aliquot of this emulsion was

gently placed on top of 400 μL of the outer solution in a new tube. With centrifugation at 18,000 × *g* for 30 min at 4 °C, emulsions passed through the oil/water interface saturated by lipids to form a bilayer structure. Approximately 100 μL of the precipitated liposome suspension was collected through a hole opened at the bottom of the tube. To obtain the stable liposome concentration, 900 μL of the outer solution was added to this suspension and centrifuged again at 18,000 × *g* for 10 min at 4 °C. Finally, 20 μL of the precipitate was collected and diluted with 250 μL of the outer solution. In the present protocol, a small fraction of negatively charged lipid (POPG) was included to obtain dispersed GUVs with high yield (39) (also see Fig. S1). We suppose repulsive force due to the charged POPG helped to disperse vesicles, whereas it was not strong enough to resist to the dielecrophoretic force inducing the pearl-chain formation.

For the control experiment, we prepared giant vesicles with the natural swelling method (Movie S7). An identical amount and ratio of lipids in chloroform was subjected to rotary evaporation to form a thin dry lipid film in the pear-shaped flask. A 1 mL aliquot of the inner solution was gently introduced to swell giant vesicles. To match the experimental condition, 500 μL of this vesicle suspension was mixed with 500 μL of the outer solution and then centrifuged at 18,000 × *g* for 30 min at 4 °C. Finally, 20 μL of the precipitate was collected and diluted with the 250 μL of the outer solution.

**Electrofusion Setup.** The observation chamber to monitor the electrofusion of GUVs was assembled as follows. Two slips of copper ribbon (5 mm in width, 0.1 mm in height, and approximately 5 cm in length) were mounted onto a 60 × 24 $mm^2$ cover glass (Matsunami Glass) with an approximate 1-mm gap using a 25-μm thick double-sided tape (8171J; 3M). The gap between the copper slips was precisely measured by a micrometer every time to adjust the electric field for fusion. These slips were connected via clips to the signal generator for cell electrofusion (LF201; Nepa Gene). After immersing the chamber in a BSA solution, an 18 × 18 $mm^2$ cover glass was glued on top with grease as a lid. The vesicle suspension was applied to the gap between the copper slips through capillary action. The resistivity of the vesicle suspension was 6 ~ 10 Ωcm. The electric signal used for vesicle alignment and fusion was explained in the main text.

**Image Acquisition.** Microscope images were obtained using an inverted light microscope (IX71; Olympus). Bright-field images were obtained through differential interference contrast observation (e.g., Fig. 1*C*), and epifluorescence images (e.g., Fig. 1 *B* and *D*) were obtained through the corresponding filter and dichroic mirror unit (U-MWIB2; Olympus; excitation 450–480 nm/emission cutoff 510 nm). In these cases, the 40 × dry objective was used and time-lapse images with 1 s intervals were obtained using a digital color charge-coupled device (CCD) camera (VB-7000; Keyence). Confocal images were obtained using a real-time laser confocal microscope unit (CSU10; Yokogawa Electric) and a cooled high-resolution digital CCD camera (iXon; Andor) with a 30 mW 488 nm Ar/Kr laser as an excitation light. A 100 × oil-immersion objective was used to obtain time-lapsed 3D confocal images (e.g., Fig. 1 *E* and *F* and Fig. S5*A*) with a 1-s exposure time.

**Evaluation of Budding Probability.** In evaluating the budding probability $P_{bud}$, we judged whether the fused vesicles formed a budded shape within 10 min by observing the recorded sequential images. Increased constriction of the vesicle and the appearance of the septum were judged to represent a budding event. We recorded time-lapse images after fusion five to 40 times for the same condition, which typically included between one and 10 vesicle fusion events in the observation area. With this procedure, we typically obtained more than 100 fusion events in each experimental condition.

**ACKNOWLEDGMENTS.** We thank Dr. T. Toyota for instruction of the vesicle formation method. We also thank Drs. M. M. Hanczyc, N. Ichihashi, and S. Tsuda for helpful discussion. This research was supported in part by Special Coordination Funds for Promoting Science and Technology: Yuragi Project, the Global Centers of Excellence Program of the Japanese Ministry of Education, Culture, Sports, Science, and Technology.

1. Segre D, Lancet D (2000) Composing life. *EMBO Rep* 1(3):217–222.
2. Chen IA (2006) GE prize-winning essay. The emergence of cells during the origin of life. *Science* 314:1558–1559.
3. Szostak JW, Bartel DP, Luisi PL (2001) Synthesizing life. *Nature* 409:387–390.
4. Luisi PL, Ferri F, Stano P (2006) Approaches to semi-synthetic minimal cells: A review. *Naturwissenschaften* 93:1–13.
5. Zepik HH, Walde P (2008) Achievements and challenges in generating protocell models. *Chembiochem* 9:2771–2772.
6. Hanczyc MM, Fujikawa SM, Szostak JW (2003) Experimental models of primitive cellular compartments: Encapsulation, growth, and division. *Science* 302:618–622.
7. Chen IA, Szostak JW (2004) A kinetic study of the growth of fatty acid vesicles. *Biophys J* 87:988–998.
8. Chen IA, Roberts RW, Szostak JW (2004) The emergence of competition between model protocells. *Science* 305:1474–1476.
9. Mansy SS, et al. (2008) Template-directed synthesis of a genetic polymer in a model protocell. *Nature* 454:122–125.
10. Wick R, Walde P, Luisi PL (1995) Light-microscopic investigations of the autocatalytic self-reproduction of giant vesicles. *J Am Chem Soc* 117:1435–1436.
11. Pohorille A, Deamer D (2009) Self-assembly and function of primitive cell membranes. *Res Microbiol* 160:449–456.
12. Deamer D, et al. (2002) The first cell membranes. *Astrobiology* 2:371–381.
13. Lonchin S, Luisi PL, Walde P, Robinson BH (1999) A matrix effect in mixed phospholipid/fatty acid vesicle formation. *J Phys Chem B* 103:10910–10916.
14. Zhu TF, Szostak JW (2009) Coupled growth and division of model protocell membranes. *J Am Chem Soc* 131:5705–5713.
15. Takakura K, Toyota T, Sugawara T (2003) A novel system of self-reproducing giant vesicles. *J Am Chem Soc* 125:8134–8140.
16. Toyota T, et al. (2008) Population study of sizes and components of self-reproducing giant multilamellar vesicles. *Langmuir* 24:3037–3044.
17. Kurihara K, et al. (2011) Self-reproduction of supramolecular giant vesicles combined with the amplification of encapsulated DNA. *Nat Chem* 3:775–781.
18. Budin I, Szostak JW (2011) Physical effects underlying the transition from primitive to modern cell membranes. *Proc Natl Acad Sci USA* 108:5249–5254.
19. Stoicheva NG, Hui SW (1994) Electrofusion of cell-size liposomes. *Biochim Biophys Acta* 1195:31–38.
20. Pantazatos DP, MacDonald RC (1999) Directly observed membrane fusion between oppositely charged phospholipid bilayers. *J Membr Biol* 170:27–38.
21. Tanaka T, Yamazaki M (2004) Membrane fusion of giant unilamellar vesicles of neutral phospholipid membranes induced by $La^{3+}$. *Langmuir* 20:5160–5164.
22. Lentz BR (2007) PEG as a tool to gain insight into membrane fusion. *Eur Biophys J* 36:315–326.
23. Chan YHM, van Lengerich B, Boxer SG (2008) Lipid-anchored DNA mediates vesicle fusion as observed by lipid and content mixing. *Biointerphases* 3:Fa17–Fa21.
24. Cypionka A, et al. (2009) Discrimination between docking and fusion of liposomes reconstituted with neuronal SNARE-proteins using FCS. *Proc Natl Acad Sci USA* 106:18575–18580.
25. Sunami T, et al. (2010) Detection of association and fusion of giant vesicles using a fluorescence-activated cell sorter. *Langmuir* 26:15098–15103.
26. Caschera F, et al. (2011) Programmed vesicle fusion triggers gene expression. *Langmuir* 27:13082–13090.
27. Luisi PL, de Souza TP, Stano P (2008) Vesicle behavior: In search of explanations. *J Phys Chem B* 112:14655–14664.
28. Macdonald RC, et al. (1991) Small-volume extrusion apparatus for preparation of large, unilamellar vesicles. *Biochim Biophys Acta* 1061:297–303.
29. Karlsson A, et al. (2001) Networks of nanotubes and containers. *Nature* 409:150–152.
30. Kä J, Sackmann E (1991) Shape transitions and shape stability of giant phospholipid-vesicles in pure water induced by area-to-volume changes. *Biophys J* 60:825–844.
31. Tanaka T, Sano R, Yamashita Y, Yamazaki M (2004) Shape changes and vesicle fission of giant unilamellar vesicles of liquid-ordered phase membrane induced by lysophosphatidylcholine. *Langmuir* 20:9526–9534.
32. Baumgart T, Hess ST, Webb WW (2003) Imaging coexisting fluid domains in biomembrane models coupling curvature and line tension. *Nature* 425:821–824.
33. Yanagisawa M, Imai M, Taniguchi T (2008) Shape deformation of ternary vesicles coupled with phase separation. *Phys Rev Lett* 100:148102.
34. Andes-Koback M, Keating CD (2011) Complete budding and asymmetric division of primitive model cells to produce daughter vesicles with different interior and membrane compositions. *J Am Chem Soc* 133:9545–9555.
35. Staneva G, Angelova MI, Koumanov K (2004) Phospholipase A(2) promotes raft budding and fission from giant liposomes. *Chem Phys Lipids* 129:53–62.
36. Miller SL (1953) A production of amino acids under possible primitive earth conditions. *Science* 117:528–529.
37. Natsume Y, Pravaz O, Yoshida H, Imai M (2010) Shape deformation of giant vesicles encapsulating charged colloidal particles. *Soft Matter* 6:5359–5366.
38. Pautot S, Frisken BJ, Weitz DA (2003) Production of unilamellar vesicles using an inverted emulsion. *Langmuir* 19:2870–2879.
39. Nishimura K, et al. (2009) Population analysis of structural properties of giant liposomes by flow cytometry. *Langmuir* 25:10439–10443.
40. Takiguchi K, et al. (2008) Entrapping desired amounts of actin filaments and molecular motor proteins in giant liposomes. *Langmuir* 24:11323–11326.
41. Hase M, Yamada A, Hamada T, Yoshikawa K (2006) Transport of a cell-sized phospholipid micro-container across water/oil interface. *Chem Phys Lett* 426:441–444.
42. Hui SW, Kuhl TL, Guo YQ, Israelachvili J (1999) Use of poly(ethylene glycol) to control cell aggregation and fusion. *Colloids Surf B Biointerfaces* 14:213–222.
43. Asakura S, Oosawa F (1954) On interaction between two bodies immersed in a solution of macromolecules. *J Chem Phys* 22:1255–1256.
44. Asakura S, Oosawa F (1958) Interaction between particles suspended in solutions of macromolecules. *J Polym Sci* 33:183–192.
45. Minton AP (2001) The influence of macromolecular crowding and macromolecular confinement on biochemical reactions in physiological media. *J Biol Chem* 276:10577–10580.

46. Zhou HX, Rivas GN, Minton AP (2008) Macromolecular crowding and confinement: Biochemical, biophysical, and potential physiological consequences. *Annu Rev Biophys* 37:375–397.
47. Seifert U, Berndl K, Lipowsky R (1991) Shape transformations of vesicles—phase-diagram for spontaneous-curvature and bilayer-coupling models. *Phys Rev A* 44:1182–1202.
48. Miao L, Seifert U, Wortis M, Döbereiner HG (1994) Budding transitions of fluid-bilayer vesicles—the effect of area-difference elasticity. *Phys Rev E Stat Nonlin Soft Matter Phys* 49:5389–5407.
49. Bar-ziv R, Moses E (1994) Instability and pearling states produced in tubular membranes by competition of curvature and tension. *Phys Rev Lett* 73:1392–1395.
50. Boal D (2002) The simplest cells. *Mechanics of the Cell* (Cambrige Univ Press, Cambrige, UK), pp 211–245.
51. Israelachvili J (1997) The different faces of poly(ethylene glycol). *Proc Natl Acad Sci USA* 94:8378–8379.
52. Döbereiner HG, Käs J, Noppl D, Sprenger I, Sackmann E (1993) Budding and fission of vesicles. *Biophys J* 65:1396–1403.
53. Tamm LK, Crane J, Kiessling V (2003) Membrane fusion: A structural perspective on the interplay of lipids and proteins. *Curr Opin Struct Biol* 13:453–466.
54. Lipowsky R, Döbereiner HG (1998) Vesicles in contact with nanoparticles and colloids. *Europhys Lett* 43:219–225.
55. Döbereiner HG, Selchow O, Lipowsky R (1999) Spontaneous curvature of fluid vesicles induced by trans-bilayer sugar asymmetry. *Eur Biophys J Biophys Lett* 28:174–178.
56. Döbereiner HG (2000) Fluctuating vesicle shapes. *Giant Vesicles*, eds PL Luisi and P Walde (Wiley, New York), pp 149–167.
57. Minton AP (1983) The effect of volume occupancy upon the thermodynamic activity of proteins-some biochemical consequences. *Mol Cell Biochem* 55:119–140.